Neutrino absorption by hot nuclei in supernova environments

Alan A. Dzhioev,[1,][*] A. I. Vdovin,[1,][†] and J. Wambach[2,3,][‡]

[1]*Bogoliubov Laboratory of Theoretical Physics, JINR, 141980 Dubna, Russia*
[2]*Institut für Kernphysik, Technische Universität Darmstadt, 64289 Darmstadt, Germany*
[3]*GSI Helmholtzzentrum für Schwerionenforschung, Planckstrasse 1, 64291 Darmstadt, Germany*

Using the thermal quasiparticle random-phase approximation, we study the process of neutrino and antineutrino capture on hot nuclei in supernova environments. For the sample nuclei ^{56}Fe and ^{82}Ge we perform a detailed analysis of thermal effects on the strength distribution of allowed Gamow-Teller (GT) transitions which dominate low-energy charged-current neutrino reactions. The finite-temperature cross sections are calculated taking into account the contributions of both allowed and forbidden transitions. The enhancement of the low-energy cross sections is explained by considering thermal effects on the $GT_{\pm}$ strength. For ^{56}Fe we compare the calculated finite-temperature cross sections with those obtained from large-scale shell-model calculations.

I. INTRODUCTION

It is well known that core-collapse supernova simulations require a detailed description of neutrino transport including all potentially important neutrino reactions [1]. Neutrinos are the mediators of the energy transfer from the core to the outer stellar layers and their luminosities and spectra are a crucial ingredient for the supernova explosion mechanism. Despite significant progress in our understanding of the core-collapse mechanism, many supernova simulations fail to produce an explosion (see, e.g., Refs. [2,3], and references therein). One of the possible reasons for this failure could be the incomplete and inaccurate treatment of the neutrino-nucleus processes occurring in supernova environments.

It was pointed out by Haxton [4] that neutral- and charged-current neutrino reactions on nuclei involving the excitation of the giant resonances might help re-energize the explosion and they should, therefore, be taken into account in supernova simulations. Such simulations were performed by Bruenn and Haxton [5] and it was shown that inelastic neutrino-nucleus scattering plays an important role in equilibrating neutrinos with matter. However, the simulations did not confirm Haxton's suggestion that neutrino-nucleus reactions might help to revive the stalled shock wave.

In Ref. [5], the nuclear composition of the core was approximated by a single representative nucleus, ^{56}Fe, and the relevant cross sections and rates were evaluated considering only allowed (Gamow-Teller) and first-forbidden upward transitions from the nuclear ground state. However, in the hot supernova environment with temperatures $T \gtrsim 1$ MeV nuclei exist as a thermal ensemble; i.e., nuclear excited states are thermally populated according to the Boltzmann distribution. As was first realized in Ref. [6], downward transitions from excited states remove the reaction threshold and can significantly enhance the reaction cross section at low neutrino energies.

From a microscopic point of view, there are two ways to treat neutrino reactions with hot nuclei. The first one involves a state-by-state summation over Boltzmann-weighted, individually determined contributions from nuclear ground and excited states. To apply this method, one needs to know the strength distribution of electroweak transition operators for thermally populated nuclear states. The second method is based on a statistical formulation of the nuclear many-body problem. In this approach, rather than computing individual strength distributions, one determines an "average" temperature-dependent strength function.

For iron-group nuclei ($A = 45$–65) the first approach was developed in Refs. [7–9] on the basis of large-scale shell-model (LSSM) diagonalization calculations. Modern high-performance computer capabilities combined with state-of-the-art diagonalization approaches are able to provide detailed strength distributions for both charge-neutral and charge-changing Gamow-Teller transitions that dominate neutrino reactions with pf-shell iron-group nuclei at low neutrino energies ($E_\nu \lesssim 20$ MeV). However, at temperatures $T \gtrsim 1$ MeV an explicit state-by-state summation over all thermally populated states presently remains computationally prohibitive. To overcome this problem the "Brink hypothesis" is applied; i.e., it is assumed that Gamow-Teller (GT) distributions on nuclear excited states are the same as for the ground state. To account for thermal effects, the giant resonances built on the ground and low-lying daughter states in the inverse reaction are considered. Such excited states are called backresonances and their importance arises from the large nuclear matrix elements and increased phase space. Thus, within LSSM calculations the temperature dependence of the cross sections is composed solely in the backresonance terms.

Within the shell-model approach it is assumed that the GT distributions on thermally excited states are the same as for the ground state. This is not likely the case as the vanishing of pairing correlations and smearing of the Fermi surface with increasing temperature should affect the distribution centroid and move it slightly down in energy. This conjecture is confirmed by shell-model Monte Carlo studies performed at finite temperature [10]. In addition, with present computer

—————
[*]dzhioev@theor.jinr.ru
[†]vdovin@theor.jinr.ru
[‡]jochen.wambach@physik.tu-darmstadt.de

capabilities the shell-model diagonalization cannot be applied for nuclei beyond the pf shell because of the huge configurational space involved. These shortcomings can be avoided in a thermal quasiparticle random-phase approximation (TQRPA). In Ref. [11], the TQRPA was proposed as a method to study the response of hot nuclei to weak external perturbations in the framework of a statistical approach. Being based on the thermofield dynamics (TFD) formalism [12–14], the TQRPA enables the computation of a temperature-dependent strength function avoiding the assumption of Brink's hypothesis. In Refs. [15,16], the TQRPA was applied to study thermal effects on neutral-current inelastic neutrino scattering on ^{54,56}Fe and neutron-rich germanium isotope ^{82}Ge. It was shown that the TQRPA reveals the same thermal effects on the cross sections as the LSSM approach. Namely, the reaction threshold for inelastic neutrino-nucleus scattering is removed at finite temperature and the cross section for low-energy neutrinos is significantly enhanced. It was found, however, that within the TQRPA the enhancement is caused by both deexcitation of nuclear excited states and thermally unblocked low-energy GT transitions. The latter do not appear within the LSSM owing to application of Brink's hypothesis. Moreover, it was shown in Ref. [15] that, unlike in the LSSM approach, the principle of detailed balance is not violated within the TQRPA and it results in a larger strength for downward GT transitions from excited states. As a consequence, at low neutrino energies the finite-temperature cross sections calculated within the TQRPA turn out to be several times larger than those obtained within the shell-model calculations.

In the present paper, we apply the TQRPA method to study thermal effects on charged-current neutrino-nucleus reactions (ν_e, e^-) and $(\bar{\nu}_e, e^+)$ occurring in the supernova environment. Here we would like to mention that the TQRPA was already applied for charge-changing reactions with hot nuclei when studying thermal effects on electron capture in supernovae [17,18]. The paper is organized as follows. In Sec. II we review the basics of the TFD formalism and outline how to treat charge-changing transitions in a hot nucleus within the TQRPA. For more details of the approach, the reader is referred to Refs. [17,18]. In addition, in Sec. II the expressions necessary to calculate cross sections for ν_e and $\bar{\nu}_e$ absorption on hot nuclei are given. The results of the numerical calculations are presented and discussed in Sec. III for the sample nuclei ^{56}Fe and ^{82}Ge. For ^{56}Fe we compare the calculated ground-state and finite-temperature cross sections with available results from other approaches. Conclusions are drawn in Sec. IV. In an Appendix we prove in a model-independent way that the principle of detailed balance is valid for charge-changing transitions if hot nuclei in the supernova environment are treated in the grand-canonical ensemble.

II. FORMALISM

During the core-collapse phase of a supernovae explosion the temperature in the iron core is sufficiently high (a few 10^9 K) to establish an equilibrium of reactions mediated by the strong and electroweak interaction [1]. Neglecting weak-interaction reactions, we can consider nuclei as open

quantum systems in thermal equilibrium with heat and particle reservoirs and, hence, they can be described as a thermal grand canonical ensemble with temperature T and proton and neutron chemical potentials λ_p and λ_n, respectively. In thermofield dynamics (TFD), such an ensemble is represented by the thermal vacuum $|0(T)\rangle$, which is a temperature-dependent state in the extended Hilbert space.[1] The thermal vacuum is determined as the zero-energy eigenstate of the thermal Hamiltonian, $\mathcal{H} = H - \widetilde{H}$, and it satisfies the thermal-state condition

$$A|0(T)\rangle = \sigma_A e^{\mathcal{H}/2T} \widetilde{A}^\dagger |0(T)\rangle. \tag{1}$$

In the above equations H is the original nuclear Hamiltonian (proton and neutron chemical potentials are included in H) and $\widetilde{H}$ is its tilde counterpart acting in the auxiliary Hilbert space; an operator A acts in the physical Hilbert space, $\widetilde{A}$ is its tilde partner, and σ_A is a phase factor. The thermal-state condition guarantees that the expectation value $\langle 0(T)|A|0(T)\rangle$ is equal to the grand-canonical average of A. In this sense, relation (1) is equivalent to the Kubo-Martin-Schwinger condition for an equilibrium grand-canonical density matrix [19].

External perturbations mediated by weak interaction induce transitions from the thermal vacuum to nonequilibrium states. Within the TDF such nonequilibrium states are given by the eigenstates of the thermal Hamiltonian $\mathcal{H}$. As follows from the definition of $\mathcal{H}$, each of its eigenstates with positive energy has a counterpart—the tilde-conjugate eigenstate—with negative but the same absolute value of energy. This gives the possibility to describe both endoergic and exoergic neutrino reactions with hot nuclei. In what follows we refer to positive-energy eigenstates as nontilde states and to negative-energy eigenstates as tilde states.

A. Thermal quasiparticle RPA

In Refs. [17,18] we introduced the proton-neutron TQRPA method which allows for a treatment of charge-changing transitions in hot nuclei induced by (anti)neutrino absorption. For the sake of completeness, let us briefly recall the method.

Within the TQRPA, nonequilibrium states of a hot nucleus caused by an external perturbation are treated as phononlike excitations on the thermal vacuum

$$\begin{aligned} |Q_{JMi}\rangle &= Q^\dagger_{JMi}|0(T)\rangle, \\ |\widetilde{Q}_{JMi}\rangle &= \widetilde{Q}^\dagger_{JMi}|0(T)\rangle, \end{aligned} \tag{2}$$

where we denote $\widetilde{Q}^\dagger_{JMi} = (-1)^{J-M} \widetilde{Q}^\dagger_{J-Mi}$. Phonon excitations are considered as the normal modes of the thermal Hamiltonian,

$$\mathcal{H} \simeq \sum_{JMi} \omega_{Ji}(T)(Q^\dagger_{JMi} Q_{JMi} - \widetilde{Q}^\dagger_{JMi} \widetilde{Q}_{JMi}), \tag{3}$$

---

[1]The correspondence between the thermofield dynamics and the so-called superoperator formalism is discussed in Ref. [20]. The latter is used by one of the authors (A.D.) to study nonequilibrium transport phenomena (see, e.g., Ref. [21]).

while the thermal vacuum $|0(T)\rangle$ itself is the vacuum for the annihilation operators Q_{JMi}, $\widetilde{Q}_{JMi}$. Thus, within the TQRPA the problem of finding the excitation spectrum of a hot nucleus is reduced to the diagonalization of the thermal Hamiltonian in terms of phonon operators such that the respective phonon vacuum obeys the thermal-state condition (1).

For charge-changing multipole transitions the phonon operators are defined as a linear superposition of creation and annihilation operators of proton-neutron thermal quasiparticle pairs,[2]

$$
\begin{aligned}
Q^{\dagger}_{JMi} = \sum_{j_p j_n} \Big\{ & \psi^{Ji}_{j_p j_n} [\beta^{\dagger}_{j_p} \beta^{\dagger}_{j_n}]^J_M + \widetilde{\psi}^{Ji}_{j_p j_p} [\widetilde{\beta}^{\dagger}_{\overline{j_p}} \widetilde{\beta}^{\dagger}_{\overline{j_n}}]^J_M \\
& + i\eta^{Ji}_{j_p j_n} [\beta^{\dagger}_{j_p} \widetilde{\beta}^{\dagger}_{\overline{j_n}}]^J_M + i\widetilde{\eta}^{Ji}_{j_p j_n} [\widetilde{\beta}^{\dagger}_{\overline{j_p}} \beta^{\dagger}_{j_n}]^J_M \\
& + \phi^{Ji}_{j_p j_n} [\beta_{\overline{j_p}} \beta_{\overline{j_n}}]^J_M + \widetilde{\phi}^{Ji}_{j_p j_n} [\widetilde{\beta}_{j_p} \widetilde{\beta}_{j_n}]^J_M \\
& + i\xi^{Ji}_{j_p j_n} [\beta_{\overline{j_p}} \widetilde{\beta}_{j_n}]^J_M + i\widetilde{\xi}^{Ji}_{j_p j_n} [\widetilde{\beta}_{j_p} \beta_{\overline{j_n}}]^J_M \Big\}.
\end{aligned}
\tag{4}
$$

In turn, thermal quasiparticles are normal modes of the pairing part of the thermal Hamiltonian

$$
\mathcal{H}_{\text{pair}} \simeq \sum_{\tau} \sum_{jm}^{\tau} \varepsilon_j(T) (\beta^{\dagger}_{jm} \beta_{jm} - \widetilde{\beta}^{\dagger}_{jm} \widetilde{\beta}_{jm}),
\tag{5}
$$

and their vacuum is the thermal vacuum in the BCS approximation. In the expression above, the notation $\sum^{\tau}$ implies a summation over neutron ($\tau = n$) or proton ($\tau = p$) single-particle states only. Thermal quasiparticles are connected with Bogoliubov quasiparticles by so-called thermal transformation,[3]

$$
\begin{aligned}
\beta^{\dagger}_{jm} &= x_j \alpha^{\dagger}_{jm} - iy_j \widetilde{\alpha}_{jm}, \\
\widetilde{\beta}^{\dagger}_{jm} &= x_j \widetilde{\alpha}^{\dagger}_{jm} + iy_j \alpha_{jm}, \quad (x_j^2 + y_j^2 = 1).
\end{aligned}
\tag{6}
$$

The (x, y) coefficients, as well as the (u, v) coefficients of the Bogoliubov transformations, are found from the finite-temperature BCS equations (see Ref. [18] for more details). In accordance with the BCS theory [22,23], the numerical solution of these equations yields vanishing pairing correlations above a certain critical temperature.

To clarify the physical meaning of different terms in Eq. (4), we note that the creation of a negative-energy tilde thermal quasiparticle corresponds to the annihilation of a thermally excited Bogoliubov quasiparticle or, which is the same, to the creation of a quasihole state (see Ref. [18] for more details). Therefore, at finite temperature, single-particle charge-changing transitions involve excitations of three types: (1) two-quasiparticle excitations described by the operator $\beta^{\dagger}_{j_p} \beta^{\dagger}_{j_n}$ and having energy $\varepsilon^{(+)}_{j_p j_n} = \varepsilon_{j_p} + \varepsilon_{j_n}$; (2) one-quasiparticle, one-quasihole excitations described by the operators $\beta^{\dagger}_{j_p} \widetilde{\beta}^{\dagger}_{j_n}$, $\widetilde{\beta}^{\dagger}_{j_p} \beta^{\dagger}_{j_n}$ and having energies $\varepsilon^{(-)}_{j_p j_n} = \varepsilon_{j_p} - \varepsilon_{j_n}$ and $-\varepsilon^{(-)}_{j_p j_n}$, respectively; and (3) two-quasihole excitations

---

described by the operator $\widetilde{\beta}^{\dagger}_{j_p} \widetilde{\beta}^{\dagger}_{j_n}$ and having energy $-\varepsilon^{(+)}_{j_p j_n}$. The last two types are possible only at $T \neq 0$. Therefore, owing to single-particle transitions involving annihilation of thermally excited Bogoliubov quasiparticles, the phonon spectrum at finite temperature contains negative- and low-energy states which do not exist at zero temperature and these "new" phonon states can be interpreted as thermally unblocked transitions between nuclear excited states.

To find the energy and the wave functions of thermal phonons, we apply the equation of motion method,

$$
\langle |\delta Q, [\mathcal{H}, Q^{\dagger}]| \rangle = \omega(T) \langle |[\delta Q, Q^{\dagger}]| \rangle,
\tag{7}
$$

under two additional constraints: (a) the phonon vacuum obeys the thermal-state condition (1) and (b) phonon operators obey Bose commutation relations. The first constraint yields the relations between phonon amplitudes

$$
\begin{aligned}
\begin{pmatrix} \widetilde{\psi} \\ \widetilde{\phi} \end{pmatrix}^{Ji}_{j_p j_n} &= \frac{y_{j_p} y_{j_n} - e^{-\omega_{Ji}/2T} x_{j_p} x_{j_n}}{e^{-\omega_{Ji}/2T} y_{j_p} y_{j_n} - x_{j_p} x_{j_n}} \begin{pmatrix} \phi \\ \psi \end{pmatrix}^{Ji}_{j_p j_n}, \\
\begin{pmatrix} \widetilde{\eta} \\ \widetilde{\xi} \end{pmatrix}^{Ji}_{j_p j_n} &= \frac{y_{j_p} x_{j_n} - e^{-\omega_{Ji}/2T} x_{j_p} y_{j_n}}{e^{-\omega_{Ji}/2T} y_{j_p} x_{j_n} - x_{j_p} y_{j_n}} \begin{pmatrix} \xi \\ \eta \end{pmatrix}^{Ji}_{j_p j_n},
\end{aligned}
\tag{8}
$$

while the last assumption is equivalent to averaging with respect to the BCS thermal vacuum in the equations of motion (7) and leads to an orthonormality condition for the amplitudes [18]. Thus, the phonon energies ω in Eq. (3) as well as the amplitudes ψ, $\widetilde{\psi}$, etc., in Eq. (4) are the solution of the proton-neutron TQRPA equations. Positive-energy solutions correspond to nontilde phonons in Eq. (3), while negative-energy solutions correspond to tilde ones. Because both the energies of thermal quasiparticles and the interaction strengths between them are temperature dependent, the spectrum of thermal phonons turns out to be temperature dependent. However, it is significant that in the zero-temperature limit the described method reduces into the standard proton-neutron QRPA.

For a given multipole charge-changing transition operator $\mathcal{T}^{(\mp)}_J$ the transition probabilities (strengths) from the thermal vacuum to thermal one-phonon states are given by the following reduced matrix elements:

$$
\begin{aligned}
\Phi^{(\mp)}_{Ji} &= |\langle Q_{Ji} \| \mathcal{T}^{(\mp)}_J \| 0(T) \rangle|^2, \\
\widetilde{\Phi}^{(\mp)}_{Ji} &= |\langle \widetilde{Q}_{Ji} \| \mathcal{T}^{(\mp)}_J \| 0(T) \rangle|^2.
\end{aligned}
\tag{9}
$$

Here the symbol $(-)$ refers to neutron-to-proton transitions (β^- channel), while $(+)$ refers to proton-to-neutron transitions (β^+ channel). It can be shown that if the transition operators $\mathcal{T}^{(-)}_J$ and $\mathcal{T}^{(+)}_J$ differ only by the isospin operator, i.e., $\mathcal{T}^{(\mp)}_J = \mathcal{T}_J t_{\mp}$, the transition probabilities to tilde and nontilde phonon states are connected as

$$
\widetilde{\Phi}^{(\mp)}_{Ji} = \exp\left(-\frac{\omega_{Ji}}{T}\right) \Phi^{(\pm)}_{Ji}.
\tag{10}
$$

In Ref. [15], a similar relation is obtained for charge-neutral transitions and it is referred to as the principle of detailed balance. However, in contrast to the case of charge-neutral transitions, the detailed balance relation (10) includes a phonon energy rather than a transition energy. The latter is the energy

---

———

[2] In Eq. (4), $[\ ]^J_M$ denotes the coupling of two single-particle angular momenta j_p, j_n to the total angular momentum J.

[3] Note that we use Ojima's [14] complex form of the thermal transformation.

transferred to the parent nucleus and, for charge-changing transitions, is given by[4]

$$E_{Ji}^{(\mp)} = \omega_{Ji} \mp \delta_{np},$$
$$\widetilde{E}_{Ji}^{(\pm)} = -E_{Ji}^{(\mp)},$$
$$(11)$$

where $\delta_{np} = \Delta\lambda_{np} + \Delta M_{np}$ and $\Delta\lambda_{np}$ is the difference between neutron and proton chemical potentials in the parent nucleus and $\Delta M_{np} = 1.293$ MeV is the neutron-proton mass splitting. It is obvious that nontilde (tilde) charge-changing phonon states do not necessarily correspond to upward (downward) transitions: Owing to δ_{np}, some nontilde (tilde) phonon states may have negative (positive) transition energy. With Eq. (11), relation (10) is rewritten as

$$\widetilde{\Phi}_{Ji}^{(\mp)} = \exp\left(-\frac{E_{Ji}^{(\pm)} \mp \delta_{np}}{T}\right)\Phi_{Ji}^{(\pm)}.$$
$$(12)$$

Thus, for each $n \to p$ ($p \to n$) upward transition with energy E there is an inverse downward transition $p \to n$ ($n \to p$) with energy $-E$ and the respective transition probabilities are connected by Eq. (12). In the Appendix we show that in this form the detailed balance for charge-changing transitions in the ensemble of hot nuclei can be derived in a model-independent way.

B. Cross sections in supernova environments

In the derivation of the (anti)neutrino absorption cross section for a hot nucleus under supernova conditions, we follow the Walecka-Donnelly formalism [24,25], which is based on the standard current-current form of the weak-interaction Hamiltonian. After a multipole expansion of the weak nuclear current the temperature-dependent differential cross section for a transition from the thermal vacuum to a thermal one-phonon state is given by

$$\frac{d\sigma_{Ji}(E_\nu, T)}{d\Omega} = \frac{(G_F \cos\theta_C)^2}{\pi} p_e^i E_e^i \{\sigma_{CL}^J + \sigma_T^J\}$$
$$\times F(\pm Z + 1, E_e)[1 - f(E_e)]. \quad (13)$$

Here and below, the upper (lower) sign refers to the neutrino (antineutrino) cross section. In the above expression, G_F is the Fermi constant for the weak interaction, θ_C is the Cabbibo angle, and E_e and p_e are the energy and momentum of the outgoing electron or positron.

In Eq. (13), the contributions, σ_{CL}^J, for the Coulomb and longitudinal components, and σ_T^J, for the transverse electric and magnetic components, are written as

$$\sigma_{CL}^J = (1 + a\cos\Theta)|\langle Ji\|\hat{M}_J\|0(T)\rangle|^2 + (1 + \cos\Theta$$
$$- 2b\sin^2\Theta)|\langle Ji\|\hat{L}_J\|0(T)\rangle|^2 + \left[\frac{E_{Ji}}{q}(1 + \cos\Theta) + c\right]$$
$$\times 2\,\mathrm{Re}\langle Ji\|\hat{L}_J\|0(T)\rangle\langle Ji\|\hat{M}_J\|0(T)\rangle^*, \quad (14)$$

$$\sigma_T^J = (1 - a\cos\Theta + b\sin^2\Theta)\left[|\langle Ji\|\hat{T}_J^{\mathrm{mag}}\|0(T)\rangle|^2\right.$$
$$+ |\langle Ji\|\hat{T}_J^{\mathrm{el}}\|0(T)\rangle|^2\right] \mp \left[\frac{E_\nu + E_e^i}{q}(1 - a\cos\Theta) - c\right]$$
$$\times 2\,\mathrm{Re}\langle Ji\|\hat{T}_J^{\mathrm{mag}}\|0(T)\rangle\langle Ji\|\hat{T}_J^{\mathrm{el}}\|0(T)\rangle^*, \quad (15)$$

where Θ is the lepton scattering angle and the notation $|Ji\rangle$ is used to denote both the nontilde and the tilde thermal one-phonon states. In the former case the transition energy $E_{Ji} = E_{Ji}^{(\mp)}$, while in the latter case $E_{Ji} = \widetilde{E}_{Ji}^{(\mp)}$. Thus, the energy of the outgoing lepton is $E_e^i = E_\nu - E_{Ji}$. The parameters a, b, and c are obtained from the relations

$$a = \frac{p_e}{E_e} = \sqrt{1 - \left(\frac{m_e c^2}{E_e}\right)^2},$$
$$b = a^2\frac{E_\nu E_e}{q^2}, \quad c = \frac{(m_e c^2)^2}{q E_e}, \quad (16)$$

and the absolute value of the three-momentum transfer q is given,

$$q = \sqrt{E_{Ji}^2 + 2E_e E_\nu(1 - a\cos\Theta) - (m_e c^2)^2}. \quad (17)$$

The multipole operators $\hat{M}_J$, $\hat{L}_J$, $\hat{J}_J^{\mathrm{el}}$, and $\hat{J}_J^{\mathrm{mag}}$ denote the charge, longitudinal, and transverse electric and magnetic parts of the hadronic current, respectively, as defined in Refs. [24,25]. For the vector, axial-vector, and pseudoscalar form factors that describe the internal structure of the nucleon we use parametrization from Ref. [26] (see also Ref. [27]).

For charged-current reactions, the cross section (13) must be corrected for the distortion of the outgoing lepton wave function by the Coulomb field of the residual (daughter) nucleus. The cross section can either be multiplied a Fermi function $F(Z, E)$ (see, e.g., Ref. [28]), or, at higher energies, the effect of the Coulomb field can be described by the effective momentum approximation (EMA) [29]. In the present study, by following the prescription from Refs. [30,31], we choose an energy point in which both approaches predict the same values. Then the Fermi function is used below the point and the EMA is adopted above it.

Furthermore, in the supernova environment nuclei are surrounded by a nearly degenerate electron gas. Thus, neutrino absorption can be strongly reduced by Pauli blocking of the final electron states. The blocking factor $[1 - f(E_e)]$ in Eq. (13) accounts for this effect, where $f(E_e)$ is the Fermi-Dirac distribution with temperature T and the chemical potential μ_{e^-}. The positron distribution is defined in the same way with $\mu_{e^+} = -\mu_{e^-}$. Therefore, we can neglect the blocking factor for antineutrino absorption.

The total cross section $\sigma(E_\nu, T)$, as a function of temperature and incoming (anti)neutrino energy, is obtained from the differential cross sections (13) by integrating over the scattering angle and summing over all possible final thermal one-phonon states,

$$\sigma(E_\nu, T) = 2\pi \sum_{Ji} \int_1^{-1} \frac{d\sigma_{Ji}}{d\Omega} d\cos\Theta$$
$$= \sigma_{\mathrm{en}}(E_\nu, T) + \sigma_{\mathrm{ex}}(E_\nu, T). \quad (18)$$

---

[4]At $T = 0$, the transition energy corresponds to the final-state energy measured from parent-nucleus ground state.

Here the total cross section is split into two parts: $\sigma_{\text{en}}(E_\nu,T)$ describes the endoergic neutrino absorption and includes only upward transitions ($E_{Ji} > 0$), while $\sigma_{\text{ex}}(E_\nu,T)$ corresponds to the exoergic process associated with downward transitions ($E_{Ji} < 0$). The contribution $\sigma_{\text{ex}}(E_\nu,T)$ dominates the cross section for vanishing neutrino energies, $E_\nu \approx 0$. It is apparent that for β-stable nuclei the exoergic absorption is only possible at finite temperatures and owing to transitions from thermally excited states.

For low-energy (anti)neutrinos, i.e., in the long wavelength limit $q \to 0$, the allowed 1^+ multipole operator reduces to the Gamow-Teller form,

$$\text{GT}_\mp = g_A \vec{\sigma} t_\mp, \tag{19}$$

where $g_A = -1.2599$ [32] is the axial weak coupling constant. Considering only GT transitions and taking into account detailed balance according to Eq. (10), the cross section (18) can be written as

$$
\begin{aligned}
&\sigma(E_\nu,T) \\
&= \frac{(G_{\text{F}}\cos\theta_{\text{C}})^2}{\pi} \\
&\quad \times \left\{ \sum_i (E_\nu - E_i^{(\mp)})^2 \Phi_i^{(\mp)} F(\pm Z + 1, E_e) \right. \\
&\quad \left. + \sum_i (E_\nu + E_i^{(\pm)})^2 \exp\left(-\frac{\omega_i}{T}\right) \Phi_i^{(\pm)} F(\pm Z + 1, E_e) \right\}.
\end{aligned}
\tag{20}
$$

Here, for simplicity, the electron rest mass has been neglected, i.e., $E_e \approx p_e$, and the blocking factor for the outgoing lepton has been dropped. The matrix elements $\Phi_i^{(\mp)}$ denote the transition strength of the $\text{GT}_\mp$ operator. The first term in Eq. (20) implies summation over nontilde 1^+ states. Within the shell-model approach this term reduces to the ground-state contribution (see Eq. (2) in Ref. [7]). However, in the TQRPA this term appears to be temperature dependent owing to a violation of Brink's hypothesis. The second term accounts for transitions to tilde states and it is an analog of the backresonance contribution within the shell-model approach. Here we would like to stress that we cannot associate transitions to nontilde (tilde) states with the endoergic (exoergic) absorption. As mentioned above, owing to δ_{np} some nontilde (tilde) states may correspond to downward (upward) transitions and, hence, contribute to σ_{ex} (σ_{en}).

III. RESULTS AND DISCUSSION

We employ the theoretical framework presented above to study thermal effects on the (ν_e,e^-) and $(\bar{\nu}_e,e^+)$ cross sections for two sample nuclei, ^{56}Fe and ^{82}Ge. The iron isotope is among the most abundant nuclei at the early stage of the core collapse, while the neutron-rich germanium isotope can be considered as the average nucleus at later stages [33].

To describe charge-changing transitions in a hot nucleus, we use the same phenomenological nuclear Hamiltonian as in Ref. [18]. The Hamiltonian consists of spherically symmetric Woods-Saxon potentials for protons and neutrons, BCS pair-

ing interactions, and separable multipole and spin-multipole residual interactions in the particle-hole channel. We neglect particle-particle interactions except for the BCS pairing forces. This Hamiltonian is usually referred to as the quasiparticle-phonon model (QPM) [34]. For the two nuclei considered, the parameters of the QPM Hamiltonian are fixed in the same manner as in Refs. [15,18]. Here we just mention that solving the BCS equations at zero temperature we get the following proton and neutron pairing gaps: $\Delta_{p(n)} = 1.57(1.36)\,\text{MeV}$ for ^{56}Fe and $\Delta_{p(n)} = 1.22(0.0)\,\text{MeV}$ for ^{82}Ge. Thus, the critical temperature ($T_{\text{cr}} \approx 0.5\Delta_\tau$) when the pairing phase transition occurs is $T_{\text{cr}} \approx 0.8\,\text{MeV}$ for the iron isotope and $T_{\text{cr}} \approx 0.6\,\text{MeV}$ for the germanium isotope.

A separable form of the residual interaction allows us to reduce the TQRPA equations to a secular equation. The explicit form for charge-changing excitations as well as expressions for transition strengths (9) are given in Refs. [17,18]. Moreover, it has been proved in Ref. [17] that the TQRPA fulfills the Ikeda sum rule for allowed Fermi and GT transitions.

A. Ground-state cross sections

As in Ref. [15], before proceeding to discuss thermal effects on neutrino-nucleus absorption cross sections, we consider the ground-state ($T = 0$) cross sections for ^{56}Fe(ν_e,e^-), ^{56}Fe($\bar{\nu}_e,e^+$), ^{82}Ge(ν_e,e^-), and ^{82}Ge($\bar{\nu}_e,e^+$) reactions and compare the our results with those available from other theoretical studies. In Fig. 1, the calculated total cross sections are shown as functions of the incident (anti)neutrino energy E_ν. We find that for $E_\nu \leqslant 100\,\text{MeV}$ the reactions considered are dominated by the multipole transitions $J^\pi \leqslant 3^\mp$, while contributions from higher multipoles are only a few percent of the total cross sections.

For ^{56}Fe the cross sections increase sharply as E_ν approaches the reaction threshold $Q_- = 4.56\,\text{MeV}$ for ν_e absorption and $Q_+ = 4.71\,\text{MeV}$ for $\bar{\nu}_e$ absorption ($Q_\mp = M_f + m_e c^2 - M_i$, where $M_{i,f}$ are the masses of the parent and daughter nuclei). As the neutron number increases, the threshold energy for ν_e absorption decreases. For the neutron-rich nucleus ^{82}Ge the Q_- value becomes negative ($Q_- = -4.71\,\text{MeV}$), allowing neutrino absorption for all energies. Contrary to this, for the ($\bar{\nu}_e,e^+$) reactions the Q_+ values become less favorable with increasing neutron excess. The antineutrino has to overcome a noticeable threshold ($Q_+ = 13.58\,\text{MeV}$) to be absorbed by ^{82}Ge and the corresponding cross section is considerably lower in comparison to the neutrino one.

In addition to the total cross sections, contributions from the 1^+ multipole channel are shown in Fig. 1. Referring to the plots in Fig. 1 for the ^{56}Fe(ν_e,e^-), ^{56}Fe($\bar{\nu}_e,e^+$), ^{82}Ge(ν_e,e^-) reactions the cross sections are dominated by allowed 1^+ transitions for energies up to $E_\nu = 30\,\text{MeV}$, with contributions from other multipoles being much smaller. In the ^{82}Ge($\bar{\nu}_e,e^+$) cross section, however, the 1^+ contribution is negligible and forbidden transitions dominate the reaction. We find that 1^- and 2^- transitions mainly contribute to the cross section for $E_\nu < 50\,\text{MeV}$.

In Fig. 1 we also analyze the effect of the full q dependent 1^+ transition operator instead of its long-wavelength limit.
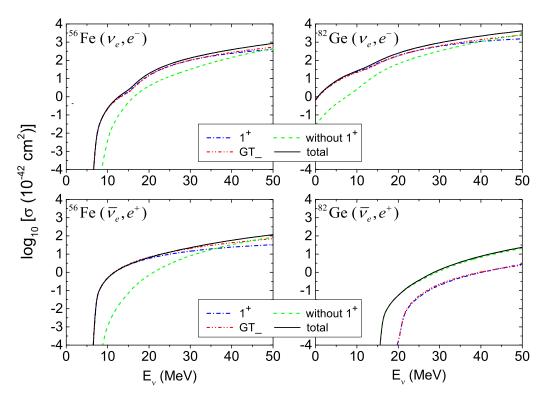
FIG. 1. (Color online) Cross sections for neutrino (top panels) and antineutrino (bottom panels) absorption reactions for ^{56}Fe and ^{82}Ge. The total cross sections (solid lines) include contributions of the $J^\pi = 0^\pm - 3^\pm$ multipoles. The dashed lines show the cross sections without the 1^+ contribution. The dash-dotted lines correspond to the 1^+ contributions calculated with the full momentum-dependent transition operator, whereas the 1^+ contributions calculated with the Gamow-Teller operator (19) are shown by the dash-double-dotted lines.

As mentioned above, in the latter case the 1^+ transition operator reduces to the Gamow-Teller operator (19) and the ground-state cross section is given by the first term in Eq. (20). It should be noted that, to make a comparison with the shell-model calculations [35,36] more transparent, we use the same quenching factor for the axial weak coupling constant, $g_A^* = 0.74 g_A$. By comparing in Fig. 1 the 1^+ and Gamow-Teller contributions to the cross sections, we conclude that for energies $E_\nu \leqslant 30$ MeV the application of the GT operators instead of the q-dependent 1^+ operator is fully justified. Therefore, we conclude that the low-energy ground-state cross sections for the ^{56}Fe(ν_e, e^-), ^{56}Fe$(\bar{\nu}_e, e^+)$, ^{82}Ge(ν_e, e^-) reactions are completely dominated by GT transitions. In contrast, all GT$_+$ transitions of are essentially blocked in ^{82}Ge. For nuclei with $Z < 40$ and $N > 40$ blocking occurs because the valence protons are in the pf shell, while the valence neutrons occupy already the next major shell (sdg shell). In the next section it will be shown, however, that thermal effects unblock GT$_+$ transitions in ^{82}Ge and for typical supernova temperatures the low-energy ^{82}Ge$(\bar{\nu}_e, e^+)$ cross sections are also dominated by the GT contributions.

In Tables I and II, we compare the calculated ground-state cross sections for (anti)neutrino absorption by ^{56}Fe to those obtained from self-consistent QRPA calculations with Skyrme forces [37] and with the hybrid approach (LSSM calculations for GT contributions and RPA for other multipoles) [35,36]. As is seen, the three models, although based on different microscopic pictures, predict rather similar neutrino absorption cross sections. We note, however, that for low energies

$(E_\nu \leqslant 40$ MeV$)$ the present results are closer to the hybrid approach results than those of Ref. [37]. It is evident that the reason why the QRPA and the hybrid approach cross sections are systematically lower than those of the Skyrme-based calculations at $E_\nu \leqslant 40$ MeV is caused by differences in the GT$_-$ strength distributions. Although the authors of Ref. [37] do not provide the GT$_-$ distribution in ^{56}Fe, it seems that the

TABLE I. Total ^{56}Fe(ν_e, e^-) cross sections for selected neutrino energies E_ν. The present QRPA results (second column) are compared with those from Ref. [37] and with the hybrid approach results [35]. The cross sections are given in units of 10^{-42} cm^2, with exponents given in parentheses.

E_ν (MeV)	QRPA	SkQRPA [37]	Hybrid [35]
10	2.39(−1)	3.63(+0)	6.61(−1)
15	2.35(+0)	1.73(+1)	6.45(+0)
20	1.91(+1)	5.26(+1)	2.93(+1)
25	6.19(+1)	1.25(+2)	7.33(+1)
30	1.34(+2)	2.33(+2)	1.40(+2)
40	3.88(+2)	5.44(+2)	3.71(+2)
50	8.47(+2)	9.83(+2)	7.98(+2)
60	1.58(+3)	1.67(+3)	1.38(+3)
70	2.61(+3)	2.59(+3)	2.42(+3)
80	3.95(+3)	3.73(+3)	3.60(+3)
90	5.53(+3)	5.07(+3)	4.98(+3)
100	7.26(+3)	6.60(+3)	6.52(+3)

TABLE II. Same as Table I, but for the ^{56}Fe$(\bar{\nu}_e, e^+)$ reaction.

E_ν (MeV)	QRPA	SkQRPA [37]	Hybrid [36]
10.0	4.92(−1)	2.95(+0)	0(+0)
12.5	1.34 (+0)	6.09(+0)	0(+0)
15.0	2.59(+0)	1.03(+1)	2(+0)
20.0	6.48(+0)	2.17(+1)	7(+0)
25.0	1.28(+1)	3.74(+1)	1.6(+1)
30.0	2.26(+1)	5.74(+1)	3.0(+1)
40.0	5.71(+1)	1.20(+2)	8.4(+1)
50.0	1.17(+2)	2.09(+2)	1.81(+2)

Skyrme-based calculations result in a larger strength below the GT$_-$ resonance compared to the other two approaches. Other possible reasons for the discrepancy could be a lower energy of the GT$_-$ resonance and a larger total GT strength obtained from the calculations with the Skyrme interaction.

Experimental results for neutrino absorption cross sections are rather limited. The KARMEN Collaboration has measured the flux-averaged ^{56}Fe$(\nu_e, e^-)^{56}$Co cross section for the neutrino spectrum from the muon decay at rest and obtained $\langle\sigma\rangle = [251 \pm 83\text{(stat.)} \pm 42\text{(syst.)}] \times 10^{-42}$ cm^2 [38]. Our result, $\langle\sigma\rangle = 223 \times 10^{-42}$ cm^2, is in excellent agreement with the experimental value. Note that the hybrid approach predicts $\langle\sigma\rangle = 240 \times 10^{-42}$ cm^2 [35], while the QRPA calculations with Skyrme forces gives $\langle\sigma\rangle = 352 \times 10^{-42}$ cm^2 [37].

For ^{56}Fe a detailed demonstration of the most important multipole contributions to neutrino absorption cross section is presented in Fig. 2 at three neutrino energies, $E_\nu = 40, 60,$ and 80 MeV. As expected, at relatively low neutrino energies ($E_\nu \lesssim 40$ MeV) the dominant contribution to the cross section originates from 1^+ transitions. With increasing
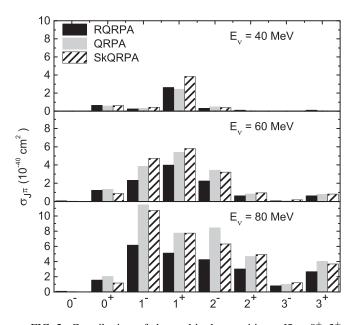

FIG. 2. Contribution of the multipole transitions $J^\pi = 0^\pm$–$3^\pm$ to the cross section for the ^{56}Fe$(\nu_e, e^-)^{56}$Co reaction at $E_\nu = 40, 60, 80$ MeV. The present QRPA results are compared with those obtained from RQRPA [39] and SkQRPA [37] calculations.

E_ν, however, contributions from other multipole transitions become important. In particular, at $E_\nu = 80$ MeV, the dominant contribution comes from 1^- transitions, but other multipoles, e.g., $1^+, 2^-, 2^+,$ and 3^+, also play an important role.

In Fig. 2, we also compare the calculated multipole decomposition of the cross section for ^{56}Fe with those from the SkQRPA calculations [37] and the relativistic QRPA (RQRPA) calculations [39]. As is evident from the figure, the latter model predicts somewhat smaller cross section at high neutrino energies ($E_\nu \gtrsim 60$ MeV), whereas we observe an excellent agreement between the results of the present QRPA and the SkQRPA. Specifically, in accordance with Refs. [37,39], we find that 0^+ allowed transitions only marginally contribute to the ^{56}Fe(ν_e, e^-) reaction. This finding is true for the other three reactions and for finite temperatures as well. For this reason, in the discussion below, we always imply 1^+ multipole channels when referring the allowed transitions.

B. Finite temperatures

In discussing ν_e and $\bar{\nu}_e$ absorption reactions under supernova conditions we follow the line of our recent work [15] and consider first thermal effects on the strength distribution of GT transitions which dominate the reactions at low energies.

In Fig. 3, we display on a logarithmic scale the GT$_-$ and GT$_+$ distributions in ^{56}Fe calculated for the ground-state ($T = 0$) and at three stellar temperatures above the critical one: $T = 0.86$ MeV (10^{10} K), 1.29 MeV (1.5×10^{10} K), and 1.72 MeV (2×10^{10} K). These temperatures roughly correspond to three stages in the collapse evolution [9]. We emphasize that the distributions are plotted with the bare GT operators $\vec{\sigma} t_\mp$ as functions of the transition energy (11). For each temperature we show the value of δ_{np} in Eq. (11) as well as the total transition strengths S_- and S_+. Note that S_- and S_+ values calculated for the ground state satisfy the Ikeda sum rule $S_- - S_+ = 3(N - Z)$ (a small deviation is caused by the incompleteness of our single-particle basis) but noticeably overestimate the experimental data ($S_- = 9.9 \pm 2.4$ [40], $S_+ = 2.9 \pm 0.3$ [41]). This overestimation is common for any QRPA calculations of GT strength and is remedied by a quenched value for the axial weak coupling constant g_A. One might notice that our QRPA calculations fairly well reproduce the experimental centroid energies for both GT$_+$ [41] and GT$_-$ [40] distributions in ^{56}Fe. In this respect the present calculations are consistent with the LSSM calculations [42]. Of course, in contrast to the LSSM approach, the QRPA cannot recover all nuclear correlations needed to reproduce the fragmentation of the GT strength.

For ^{56}Fe, owing to a relatively small absolute value of δ_{np}, the major part of the upward (downward) GT strength corresponds to transitions to nontilde (tilde) phonon states. According to our QRPA calculations, the principal contribution to the GT$_-$ (GT$_+$) strength in ^{56}Fe comes from the $1f_{7/2} \rightarrow 1f_{5/2}$ neutron-to-proton (proton-to-neutron) single-particle transition which forms a resonance peak at $E \approx 14$ MeV (≈ 6 MeV). Because the Brink hypothesis is not valid within the TQRPA, we observe an evolution of the GT resonances with temperature. Namely, when the temperature is increased to 0.86 MeV, the transition energy is lowered
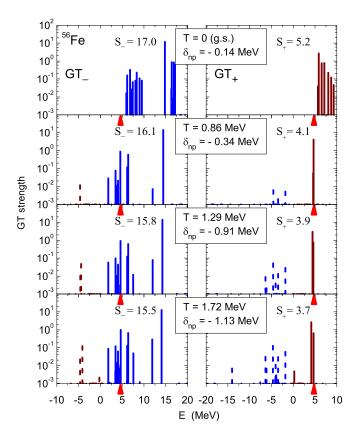
FIG. 3. (Color online) Temperature evolution of GT$_-$ (left panels) and GT$_+$ (right panels) strength distributions for ^{56}Fe vs transition energy. The solid (dashed) lines refer to transitions to nontilde (tilde) thermal one-phonon states. The arrows indicate the ground-state reaction thresholds for neutrino ($Q_- = 4.56$ MeV) and antineutrino ($Q_+ = 4.71$ MeV) absorption.

FIG. 4. (Color online) Same as Fig. 3, but for ^{82}Ge. Owing to Pauli blocking of allowed $p \to n$ transitions, the total GT$_-$ strength is many times larger than the GT$_+$ strength and $S_- \approx 3(N - Z) = 54$.

by $\sim$1.2 MeV for the GT$_-$ resonance and $\sim$2.1 MeV for the GT$_+$ resonance. This decrease in energy is mainly attributed to the vanishing of pairing correlations: At temperatures above the critical one no extra energy is needed to break a proton (neutron) Cooper pair and as a consequence the GT$_+$ (GT$_-$) resonance moves to lower energies. However, not only pairing effects lead to downward shift of the GT resonances. It can be easily seen from the structure of the TQRPA equations [17] that quasiparticle thermal occupations factors will appear which screen the interaction term. Owing to the thermal blocking of the proton-neutron repulsive residual interaction, a further increase in temperature to 1.72 MeV decreases the GT$_-$ and GT$_+$ resonances in ^{56}Fe by $\sim$0.3 and $\sim$0.5 MeV, respectively. As mentioned in the Introduction, the observed downward shift of the GT strength is not present in LSSM calculations which are partially based on Brink's hypothesis. In contrast, the finite-temperature relativistic QRPA calculations in Ref. [43] and shell-model Monte Carlo calculations in Ref. [10] show similar features for the changes of the GT resonance energy.

Finite temperature also affects the low-energy GT$_-$ strength in ^{56}Fe: Owing to the gradual disappearance of pairing, it partially shifts below the ground-state reaction threshold and becomes more fragmented. The fragmentation arises from the thermal smearing of the nuclear Fermi surface that unblocks
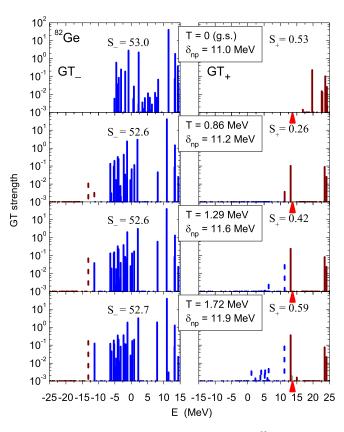
low-energy particle-particle and hole-hole GT$_-$ transitions. Here particle (hole) denotes a state above (below) the Fermi level. Moreover, in accordance with detailed balance (12), the temperature rise exponentially increases the strength of negative-energy downward transitions. Referring to the figure, the dominant part of the downward GT$_-$ strength around $E \approx -4.1$ MeV originates from a transition inverse to the GT$_+$ resonance, that is, owing to the transition from the thermally populated neutron orbit $1f_{5/2}$ to the lower lying proton orbit $1f_{7/2}$. In contrast, transitions inverse to the GT$_-$ resonance are suppressed by the energy-dependent exponent in Eq. (12) and the GT$_+$ downward strength is dominated by transitions inverse to low-energy GT$_-$ transitions. It should be mentioned that although thermal effects unblock some new GT transitions, the total GT$_\mp$ strength in ^{56}Fe slightly decreases with temperature. Nevertheless, the TQRPA preserves the Ikeda sum rule.

It is obvious that the violation of Brink's hypothesis should affect the downward GT strength. In Ref. [15], this influence was studied thoroughly for charge-neutral GT transitions in ^{56}Fe by comparing the GT running sums derived with and without Brink's hypothesis. Applying the same method, we find that both the shift of the GT$_+$ resonance to lower energies and the thermal unblocking of low-lying GT$_-$ strength enhance the GT$_-$ and GT$_+$ downward strengths in ^{56}Fe.

Figure 4 shows the temperature evolution of the GT strength function for the neutron-rich nucleus ^{82}Ge. The distributions

are displayed at the same temperatures as those for ^{56}Fe in Fig. 3. As evident from the figure, some GT strength associated with nontilde (tilde) phonon states appears at negative (positive) transition energies, which is attributable to a large value of δ_{np}. The temperature rise affects the GT$_-$ and GT$_+$ distributions in a different way. For the GT$_-$ distribution, a temperature increase essentially affects only the downward part, yielding some new strength below -10 MeV. By comparing the left and right panels in Fig. 4, we conclude that this thermally unblocked strength corresponds to transitions inverse to the GT$_+$ resonance. The GT$_-$ resonance is weakly sensitive to thermal effects. By increasing the temperature to $T = 1.72$ MeV, the excitation energy gets only lowered by ~ 0.5 MeV. Because there are no neutron pairing correlations in ^{82}Ge, this lowering is solely caused by the softening of the residual interaction.

In contrast, thermal effects are significant for the GT$_+$ resonance and they clearly demonstrate a violation of the Brink hypothesis within the TQRPA. Namely, with rising temperature the resonance peak shifts by ~ 7 MeV to lower energies and the total GT$_+$ strength shows a nonmonotomic dependence: After an initial decrease, it gradually increases. In Ref. [18], a detailed investigation within the TQRPA approach was performed on thermal effects on the GT$_+$ strength in the neutron-rich nucleus ^{76}Ge. The conclusions remain valid for ^{82}Ge as well. Briefly, for neutron-rich nuclei with $N > 40$ and $Z < 40$ the independent particle model predicts that all GT$_+$ transitions of valence protons are Pauli blocked owing to the complete occupation of the pf neutron orbits. However, both thermal excitations and pairing correlations promote protons to the sdg shell and make $1g^p_{9/2} \rightarrow 1g^n_{7/2}$ particle-particle transition in ^{82}Ge possible. The important point is that the transition energy drastically decreases with temperature. Namely, at $T < T_{cr}$, when pairing correlations are important, the transition energy is given by $\varepsilon_{1g^n_{7/2}} + \varepsilon_{1g^p_{9/2}} + \delta_{pn} \approx 20$ MeV, while at $T > T_{cr}$, when thermal effects become significant, it is given by $\varepsilon_{1g^n_{7/2}} - \varepsilon_{1g^p_{9/2}} + \delta_{pn} \approx 13$ MeV. In addition, the transition strength below the GT$_+$ resonance becomes increasingly unblocked with temperature. In particular, a strong peak owing to the $1f^p_{7/2} \rightarrow 1f^n_{5/2}$ hole-hole transition appears at $E \approx 11$ MeV. Both unblocking mechanisms are severely suppressed in the vicinity of the critical temperature ($T_{cr} \approx 0.6$ MeV in ^{82}Ge), i.e., when pairing correlations vanish while thermal effects are not yet sufficiently strong to significantly occupy the $1g_{9/2}$ proton orbit or unblock the $1f_{5/2}$ neutron orbit. Therefore, the total GT$_+$ strength decreases at $T \approx T_{cr}$. The thermal effects on the GT$_+$ strength in neutron-rich nuclei discussed here were predicted in Ref. [33] and also confirmed in Ref. [43] by calculations based on the finite-temperature relativistic QRPA. We also note that, owing to the large δ_{np}, downward GT$_+$ transitions appears to be highly suppressed in ^{82}Ge.

Let us now illustrate the influence of the thermal effects discussed above on the neutrino and antineutrino absorption by ^{56}Fe and ^{82}Ge. In Fig. 5, we compare the (ν_e, e^-) ground-state cross sections with those calculated at the three core-collapse temperatures. For energies $E_\nu < 30$ MeV, which are typical for supernova neutrinos, the cross sections are dominated by
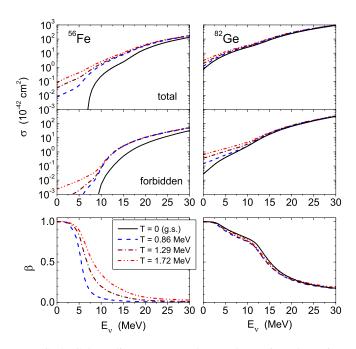

FIG. 5. (Color online) (Top panels) Total neutrino absorption cross sections for ^{56}Fe and ^{82}Ge at three different temperatures relevant for core collapse. For comparison, the ground-state cross sections are also shown. (Middle panels) Contributions from forbidden transitions to the cross sections. (Bottom panels) Temperature dependence of the ratio of exoergic absorption to the reaction cross section.

allowed GT$_-$ transitions at all temperatures. This is verified in the middle panels of Fig. 5, where the overall contribution of forbidden transitions to the finite-temperature cross sections is given. Although the forbidden cross section increases with temperature, it contributes less than 30% all the way up to $E_\nu = 30$ MeV. The bottom panels of Fig. 5 show the ratio of exoergic absorption to the reaction cross section

$$\beta(E_\nu, T) = \frac{\sigma_{ex}(E_\nu, T)}{\sigma(E_\nu, T)}, \qquad (21)$$

where $\sigma_{ex}(E_\nu, T)$ only accounts for negative-energy downward transitions induced by neutrino absorption.

When considering the ^{56}Fe(ν_e, e^-) cross section, we observe that thermal effects are unimportant for $E_\nu > 20$ MeV, i.e., when incoming neutrinos have sufficiently large energy to excite the GT$_-$ resonance. Note that a downward shift of the GT$_-$ resonance only marginally affects the cross section at such high neutrino energies. Thermal effects become pronounced though for lower neutrino energies because finite temperature removes the reaction threshold and significantly enhances the cross section. For energies $E_\nu < 5$ MeV, the ratio $\beta > 0.5$ and, hence, the observed enhancement is mostly caused by downward GT$_-$ transitions from nuclear excited states. Moreover, for $E_\nu \approx 0$ the thermally unblocked downward transitions completely dominate the reaction, increasing the cross section by more than an order of magnitude when the temperature rises from 0.86 to 1.72 MeV. The role of the exoergic absorption decreases with increasing neutrino energy and for intermediate energies, 5 MeV $< E_\nu < 20$ MeV, thermal effects on the GT$_-$
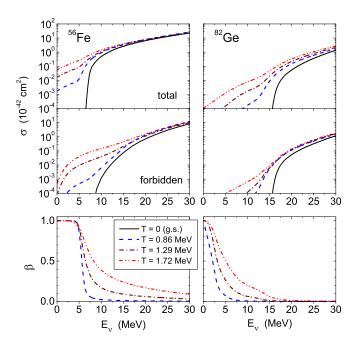
FIG. 6. (Color online) The same as in Fig. 5, but for the antineutrino absorption reaction.

FIG. 7. (Color online) Relative contribution σ_i/σ of the ith negative-energy GT state to the finite-temperature cross section at $E_\nu = 0$.

resonance and its low-energy tail become important for the cross-section enhancement.

Referring to the right panels in Fig. 5, it is shown that the ^{82}Ge(ν_e,e^-) cross section to a much lesser extent depends on temperature than that for the ^{56}Fe(ν_e,e^-) reaction. This result can be understood as follows. In ^{82}Ge, owing to the negative Q_- value, the downward GT$_-$ transitions dominate the ground-state reaction up to $E_\nu \approx 15$ MeV. As discussed above, the GT$_-$ distribution in ^{82}Ge is little affected by the temperature rise, which merely causes some additional strength at $E < -10$ MeV. This thermally unblocked downward strength becomes competitive with the ground-state contribution only at rather low energies ($E_\nu \lesssim 5$ MeV). As a result, thermal effects on the ^{82}Ge(ν_e,e^-) reaction are noticeably milder than in the previous case and a temperature rise from $T = 0$ to 1.72 MeV enhances the low-energy cross section only by a factor of about four. This observation is in line with Ref. [7], where it was shown that the thermal enhancement of the neutrino absorption cross section is reduced the more neutron-rich the nucleus is.

The results for $\overline{\nu}_e$ absorption are shown in Fig. 6. For the ^{56}Fe$(\overline{\nu}_e,e^+)$ reaction the cross section demonstrates the same trend as discussed above for the neutrino absorption by ^{56}Fe: (i) The gap in the cross section disappears and the low-energy cross section increases with temperature. (ii) With increasing E_ν the cross sections at different temperatures converge; i.e., thermal effects become unimportant. From the bottom left panel we conclude that a significant enhancement of the low-energy cross section relative to ground-state calculations comes from the increasing contribution of downward GT$_-$ transitions from nuclear excited states. The ratio β gradually reduces at $E_\nu > 5$ MeV, because at those energies the excitation of the GT$_+$ resonance becomes possible. However, at $T = 1.72$ MeV the exoergic component of the cross section
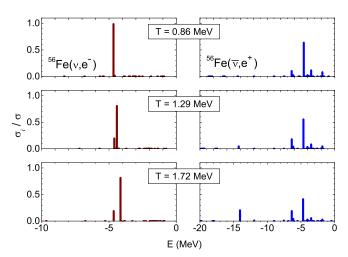
appears to be comparable with the endoergic one up to $E_\nu \approx 15$ MeV.

It should be noted that although the calculated ^{56}Fe(ν_e,e^-) and ^{56}Fe$(\overline{\nu}_e,e^+)$ cross sections show the same trend; the observed thermal enhancement at low energies is caused by different types of downward transitions. To show that, we have calculated the relative contribution σ_i/σ of different negative-energy GT states to the cross section at $E_\nu = 0$. The results are depicted in Fig. 7. As indicated in the figure, the ν absorption is completely dominated by the thermally unblocked transition inverse to the GT$_+$ resonance. For the $\overline{\nu}$ absorption, however, the main contribution to the reaction is given by transitions inverse to the GT$_-$ low-energy strength, while the "inverse" GT$_-$ resonance is suppressed by the Boltzmann factor in Eq. (20). Only at $T = 1.72$ MeV, the inverse GT$_-$ resonance gives a noticeable contribution to the absorption of low-energy antineutrinos.

As illustrated in the right panels of Fig. 6, the low-energy ^{82}Ge$(\overline{\nu}_e,e^+)$ cross section at finite temperature is also predominantly mediated by GT$_+$ transitions. Although the cross section remains substantially smaller as compared with the other three reactions considered, it demonstrates a strong temperature dependence for antineutrinos with $E_\nu < 15$ MeV, i.e., below the ground-state reaction threshold. Because the downward GT$_+$ transitions are suppressed in ^{82}Ge, the cross section enhancement reflects the thermal unblocking of the upward GT$_+$ strength. Because of the thermal unblocking, the energy below which the GT$_+$ contribution is more than half of the total cross section shifts to higher values: At $T = 0.86$ MeV this energy about 15 MeV, at $T = 1.29$ MeV it is about 20 MeV, and at $T = 1.72$ MeV it is about 25 MeV. For higher energies, forbidden transitions dominate the process like at $T = 0$ and the cross-section depends only weakly on temperature.

As mentioned above, during the core contraction neutrino absorption by nuclei is hindered by Pauli blocking of the phase space for the outgoing electron. To study this effect within the TQRPA, following Ref. [7], we
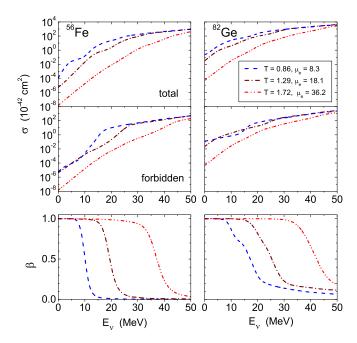
FIG. 8. (Color online) The same as in Fig. 5, but now including the outgoing electron blocking.

FIG. 9. (Color online) Comparison of the cross sections of neutrino absorption on the hot nucleus ^{56}Fe calculated within the TQRPA and the LSSM approach (see Ref. [7], Fig. 1). The cross sections in the top (bottom) panel are derived without (with) the final-state electron blocking. The respective temperatures and chemical potentials are given in MeV.

have calculated the ν absorption cross sections by introducing a blocking factor $[1 - f(E_e)]$ defined at three different sets of temperature and chemical potential (μ_e in MeV): $(T, \mu_e) = (0.86, 8.3)$, $(1.29, 18.1)$, and $(1.72, 36.2)$. The results are shown in Fig. 8 for the ^{56}Fe(ν_e, e^-) and ^{82}Ge(ν_e, e^-) reactions. As can be seen, the neutrino absorption cross sections are drastically reduced owing to electron blocking in the final state. Moreover, as the chemical potential increases faster than the temperature, the cross sections decrease with temperature. It is obvious that the absorbtion owing to deexcitation of thermally excited states is less affected by the Pauli blocking because the outgoing electron gains energy. This is clearly demonstrated by the plots in the bottom panels of Fig. 8, where the relative contribution of negative-energy transitions is shown. We thus conclude that, owing to the blocking effect, negative-energy transitions dominate the cross sections up to neutrino energies $E_\nu \gtrsim \mu_e$. Another consequence of the blocking is that downward $1\hbar\omega$ forbidden transitions become important with increasing μ_e. Without Pauli blocking their contribution in negligible owing to a small Boltzmann weight. However, as shown in the middle panels of Fig. 8, for $(T, \mu_e) = (1.29, 18.1)$ and $(1.72, 36.2)$ their contribution is comparable or even larger than those of the allowed transitions. According to our calculations, this downward forbidden contribution is mainly attributable to $0^-, 1^-, 2^-$ transitions.

In Fig. 9, the ^{56}Fe(ν_e, e^-) cross sections are displayed together with the results of the LSSM calculations (see Fig. 1 in Ref. [7]). Even if the general behavior of the cross sections as functions of the neutrino energy and temperature is in agreement in both approaches, the TQRPA results are noticeable larger than the LSSM ones but the discrepancy reduces with increasing neutrino energies. To understand the cause of the discrepancy, let us consider first the cross sections calculated
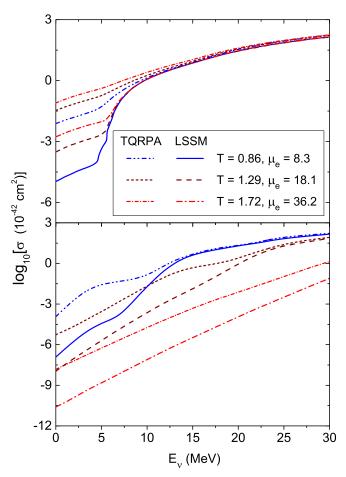
neglecting the final-state electron blocking. For $E_\nu < 5$ MeV the TQRPA cross sections exceed the LSSM values by two to three orders of magnitude. For such low energies, in both approaches, the neutrino absorption on ^{56}Fe is dominated by GT$_-$ downward transitions from thermally excited states. The differences in the description of such transitions explain the differences between the TQRPA and shell-model results. As the TQRPA is based on the grand-canonical ensemble, the upward and downward GT$_\pm$ strengths are connected by the detailed balance. As shown in Fig. 7, the absorption of low-energy neutrinos on ^{56}Fe is dominated by the downward GT$_-$ transition inverse to the GT$_+$ resonance. This corresponds to an excitation energy $\omega_i \approx 6$ MeV in the Boltzmann factor of Eq. (20). Within the shell-model calculations, downward transitions are included by backresonances, that is by inverting the GT$_+$ strength distribution of the daughter nucleus. In Ref. [7], the backresonances are built on the lowest states of ^{56}Co and the bulk of the backresonance strength in ^{56}Fe is located at an excitation energy of $E_i \approx 7$–9 MeV. This excitation energy is somewhat higher than ω_i. Moreover, within the TQRPA the downward strength concentrates in a

single state, while the shell-model GT$_+$ strength for ^{56}Co is highly fragmented owing to multinucleon correlations [44]. It is clear that both of these factors suppress the contribution of downward transitions within the LSSM. To see whether the TQRPA reliably predicts the strength of negative-energy transitions, one must go beyond the TQRPA. For a separable residual interaction used here this can be done following the method developed within the QPM, that is by taking phonon coupling into account. However, we should note that, owing to violation of Brink's hypothesis, some backresonances built on high-lying excited states of ^{56}Co may be located at the same energies as those built on the nuclear ground and low-lying states. Owing to an increasing density of states, the contribution of such backresonance states may be substantial and, therefore, their inclusion into the shell-model calculations may improve the agreement between the TQRPA and shell-model results. For $5 < E_\nu < 15$ MeV, thermally unblocked low-energy GT$_-$ transitions come into play, and because such transitions do not appear within the shell-model-based calculation, they also cause the excess of the TQRPA cross sections over the LSSM ones. At $E_\nu > 15$ MeV, ν absorption is dominated by the strong transition involving the GT$_-$ resonance. With increasing E_ν, the cross section becomes insensitive to the energy dependence of the GT distribution and depends only on the total GT$_-$ strength. As a result, we observe excellent agreement between the results of both approaches.

Comparing the cross sections calculated with Pauli blocking for the outgoing electron (see the bottom panel of Fig. 9), we note that in Ref. [7], only allowed GT$_-$ transitions are taken into account when calculating neutrino absorption cross section. As is shown in Fig. 8, if the Pauli blocking is taken into account, forbidden downward transition becomes important with increasing temperature and electron chemical potential. It is apparent that such transitions along with the above-discussed reasons lead to larger values for the TQRPA cross sections as compared to the shell-model results.

IV. CONCLUSION

In this work, we have studied thermal effects on the (anti)neutrino absorption for hot nuclei in supernova environments. For this purpose, we have employed the proton-neutron QRPA extended to finite temperatures within the TFD formalism. As an example, cross sections were calculated for ^{56}Fe and ^{82}Ge in the temperature range from $T = 0$ to 1.72 MeV by taking into account the relevant charge-exchange transitions $J^\pi = 0^\pm, 1^\pm, 2^\pm$, and $3^\pm$.

A detailed analysis of thermal effects was performed for allowed GT transitions which dominate the cross sections for $E_\nu < 30$ MeV neutrinos. Because the TQRPA does not support the Brink hypothesis, new peaks appear in the GT$_\mp$ strength function at finite temperature owing to transitions from the excited states. Moreover, thermal effects shift the GT resonance centroids to lower energies and this effect appears more strongly for the GT$_+$ strength in ^{82}Ge. The downward transitions from nuclear excited states were included in our calculations through detailed balance. The validity of detailed balance for charge-exchange transitions is a consequence of the grand-canonical treatment of hot nuclei.

We have found that thermal effects on the GT strength enhance the absorption cross sections for low-energy (anti)neutrinos by several orders of magnitude. This enhancement is mainly attributable to increasing contributions of downward transitions from excited states. However, in the supernova environment the electron chemical potential increases more rapidly than temperature. As a result, if the electron blocking in the final state is taken into account, the neutrino cross sections are drastically reduced.

Although our calculations reveal the same thermal effects as the shell-model calculation, the calculated low-energy cross sections for ^{56}Fe exceed the shell-model values by two to three orders of magnitude. One of the possible reason for this discrepancy is that the TQRPA underestimates multinucleon correlations, which are responsible for the GT strength fragmentation. However, the inclusion of backresonances built on highly excited daughter states into shell-model calculations may also improve the agreement between the TQRPA and shell-model results.

Because the TQRPA is not restricted by iron-group nuclei, it has some advantages over shell-model calculations. To enhance its reliability and predictive power, several improvements could be made. First of all, to account for multiconfigurational effects, the coupling of thermal charge-exchange phonons with more complex (e.g., two-phonon) configurations should be included into the approach. At zero temperature, this problem was considered within the QPM [45,46] by exploiting a separable form of the residual interaction. The other direction of the improvement is to combine the TQRPA method with self-consistent QRPA calculations based on either the relativistic or Skyrme nuclear energy density functionals. Recently, such calculations were performed at zero temperature [37,39]. With a separable approximation for the Skyrme interaction [47] it will be possible to calculate the phonon coupling at $T \neq 0$ within a self-consistent theory. This is planned for the future.

APPENDIX

Here we show that the detailed balance condition in the form (12) can be derived in a model-independent way. When considering a grand-canonical ensemble of hot nuclei, the probability to find the ith excited state of a nucleus with Z protons and N neutrons is given by

$$P\left(\varepsilon_i, A_N^Z\right) = (2J_i + 1) \exp\left\{-\frac{\varepsilon_i - \lambda_n N - \lambda_p Z}{T}\right\} \mathcal{Z}^{-1},$$
$$(A1)$$

where $\mathcal{Z}$ is the partition function of the grand-canonical ensemble and J_i is the angular momentum. Notice that the excitation energies ε_i are counted from the energy of noninteracting nucleons; i.e., ε_0 is a ground-state binding energy and the chemical potentials $\lambda_{n,p}$ do not include nucleon rest mass. Let us now introduce the temperature-dependent

strength function for charge-exchange transitions as a thermal average of all transition strengths (probabilities) from states in the parent nucleus to states in the daughter nucleus:

$$\Phi^{(\mp)}(E) = \sum_{Z,N} \sum_{i,f} P(\varepsilon_i, A_N^Z) S_{if}^{(\mp)} \delta(E - Q_{if}^{(\mp)}). \quad \text{(A2)}$$

Here $Q_{if}^{(\mp)} = \varepsilon_f - \varepsilon_i \mp \Delta M_{np}$ and

$$S_{if}^{(\mp)} = \left| \langle f, A_{N\mp1}^{Z\pm1} \| \mathcal{T}^{(\mp)} \| i, A_N^Z \rangle \right|^2 \quad \text{(A3)}$$

is the reduced transition strength between states i and f in the parent and daughter nuclei, respectively. In the above equations the upper sign corresponds to $n \to p$ transitions, while the lower sign refers to $p \to n$ transitions. The transition energy E can be both positive and negative.

For the transition operators $\mathcal{T}^{(-)}$ and $\mathcal{T}^{(+)}$, which differ only by the isospin operator, the respective transition strengths, $S_{if}^{(-)}$ and $S_{fi}^{(+)}$, are connected by detailed balance through

$$(2J_i + 1)S_{if}^{(-)} = (2J_f + 1)S_{fi}^{(+)}. \quad \text{(A4)}$$

Combining this result with Eq. (A2), we get the following relationship between the strength functions for $n \to p$ and $p \to n$ transitions in the thermal grand-canonical ensemble

$$\Phi^{(\pm)}(-E) = \Phi^{(\mp)}(E) \exp\left\{ -\frac{E \mp (\Delta\lambda_{np} + \Delta M_{np})}{T} \right\}. \quad \text{(A5)}$$

This relation is exactly the same as derived within the TQRPA approach for charge-changing transitions in hot nuclei.

[1] H.-T. Janka, K. Langanke, A. Marek, G. Martínez-Pinedo, and B. Müller, Phys. Rep. **442**, 38 (2007), the Hans Bethe Centennial Volume 1906–2006.

[2] M. Liebendoerfer, arXiv:astro-ph/0405029v1.

[3] A. Mezzacappa, arXiv:astro-ph/0410085v1.

[4] W. C. Haxton, Phys. Rev. Lett. **60**, 1999 (1988).

[5] S. W. Bruenn and W. C. Haxton, Astrophys. J. **376**, 678 (1991).

[6] G. M. Fuller and B. S. Meyer, Astrophys. J. **376**, 701 (1991).

[7] J. Sampaio, K. Langanke, and G. Martínez-Pinedo, Phys. Lett. B **511**, 11 (2001).

[8] J. Sampaio, K. Langanke, G. Martínez-Pinedo, and D. Dean, Phys. Lett. B **529**, 19 (2002).

[9] A. Juodagalvis, K. Langanke, G. Martínez-Pinedo, W. Hix, D. Dean, and J. Sampaio, Nucl. Phys. A **747**, 87 (2005).

[10] P. B. Radha, D. J. Dean, S. E. Koonin, K. Langanke, and P. Vogel, Phys. Rev. C **56**, 3079 (1997).

[11] A. A. Dzhioev and A. I. Vdovin, Int. J. Mod. Phys. E **18**, 1535 (2009).

[12] Y. TakahashI and H. Umezawa, Int. J. Mod. Phys. B **10**, 1755 (1996).

[13] H. Umezawa, H. Matsumoto, and M. Tachiki, *Thermo Field Dynamics and Condensed States* (North-Holland, Amsterdam, 1982).

[14] I. Ojima, Ann. Phys. **137**, 1 (1981).

[15] A. A. Dzhioev, A. I. Vdovin, J. Wambach, and V. Y. Ponomarev, Phys. Rev. C **89**, 035805 (2014).

[16] A. Dzhioev, A. Vdovin, V. Ponomarev, and J. Wambach, Phys. At. Nucl. **74**, 1162 (2011).

[17] A. Dzhioev, A. Vdovin, V. Ponomarev, and J. Wambach, Phys. At. Nucl. **72**, 1320 (2009).

[18] A. A. Dzhioev, A. I. Vdovin, V. Y. Ponomarev, J. Wambach, K. Langanke, and G. Martínez-Pinedo, Phys. Rev. C **81**, 015804 (2010).

[19] R. Kubo, J. Phys. Soc. Jpn. **12**, 570 (1957); P. C. Martin and J. Schwinger, Phys. Rev. **115**, 1342 (1959).

[20] M. Schmutz, Z. Phys. B: Condens. Matter **30**, 97 (1978).

[21] A. A. Dzhioev and D. S. Kosov, J. Phys.: Condens. Matter **24**, 225304 (2012).

[22] A. L. Goodman, Nucl. Phys. A **352**, 30 (1981).

[23] O. Civitarese, G. Dussel, and R. P. J. Perazzo, Nucl. Phys. A **404**, 15 (1983).

[24] J. D. Walecka, in *Muon Physics V2: Weak Interactions*, edited by V. W. Hughes and C. S. Wu (Elsevier Science, Amsterdam, 1975), p. 113.

[25] T. W. Donnelly and R. D. Peccei, Phys. Rep. **50**, 1 (1979).

[26] S. Singh, Nucl. Phys. B, Proc. Suppl. **112**, 77 (2002).

[27] H. Đapo and N. Paar, Phys. Rev. C **86**, 035804 (2012).

[28] K. Langanke and G. Martínez-Pinedo, Nucl. Phys. A **673**, 481 (2000).

[29] J. Engel, Phys. Rev. C **57**, 2004 (1998).

[30] C. Volpe, N. Auerbach, G. Colò, T. Suzuki, and N. Van Giai, Phys. Rev. C **62**, 015501 (2000).

[31] N. Paar, D. Vretenar, T. Marketin, and P. Ring, Phys. Rev. C **77**, 024608 (2008).

[32] I. S. Towner, in *Symmetries and Fundamental Interactions in Nuclei*, edited by W. C. Haxton and E. M. Henley (World Scientific, Singapore, 1995), p. 183.

[33] J. Cooperstein and J. Wambach, Nucl. Phys. A **420**, 591 (1984).

[34] V. G. Soloviev, *Theory of Atomic Nuclei: Quasiparticles and Phonons* (Taylor & Francis, London, 1992).

[35] E. Kolbe and K. Langanke, Phys. Rev. C **63**, 025802 (2001).

[36] J. Toivanen, E. Kolbe, K. Langanke, G. Martínez-Pinedo, and P. Vogel, Nucl. Phys. A **694**, 395 (2001).

[37] R. Lazauskas and C. Volpe, Nucl. Phys. A **792**, 219 (2007).

[38] R. Maschuw, Prog. Part. Nucl. Phys. **40**, 183 (1998).

[39] N. Paar, T. Suzuki, M. Honma, T. Marketin, and D. Vretenar, Phys. Rev. C **84**, 047305 (2011).

[40] J. Rapaport, T. Taddeucci, T. Welch, C. Gaarde, J. Larsen, D. Horen, E. Sugarbaker, P. Koncz, C. Foster, C. Goodman, C. Goulding, and T. Masterson, Nucl. Phys. A **410**, 371 (1983).

[41] S. El-Kateb, K. P. Jackson, W. P. Alford, R. Abegg, R. E. Azuma, B. A. Brown, A. Celler, D. Frekers, O. Häusser, R. Helmer, R. S. Henderson, K. H. Hicks, R. Jeppesen, J. D. King, G. G. Shute, B. M. Spicer, A. Trudel, K. Raywood, M. Vetterli, and S. Yen, Phys. Rev. C **49**, 3128 (1994).

[42] E. Caurier, K. Langanke, G. Martínez-Pinedo, and F. Nowacki, Nucl. Phys. A **653**, 439 (1999).

[43] Y. F. Niu, N. Paar, D. Vretenar, and J. Meng, Phys. Rev. C **83**, 045807 (2011).

[44] K. Langanke and G. Martínez-Pinedo, Phys. Lett. B **453**, 187 (1999).

[45] V. A. Kuzmin and V. G. Soloviev, J. Phys. G: Nucl. Phys. **10**, 1507 (1984).

[46] V. A. Kuzmin and V. G. Soloviev, J. Phys. G: Nucl. Phys. **11**, 603 (1985).

[47] N. Van Giai, C. Stoyanov, and V. V. Voronov, Phys. Rev. C **57**, 1204 (1998).